Published in final edited form as:
J Mol Biol. 2014 May 29; 426(11): 2183–2198. doi:10.1016/j.jmb.2014.03.014.

APE1 incision activity at abasic sites in tandem repeat sequences

Mengxia Li[1,*], **Jens Völker**[2], **Kenneth J. Breslauer**[2,3], and **David M. Wilson III**[1,#]

[1]Laboratory of Molecular Gerontology, National Institutes of Health, National Institute on Aging, Intramural Research Program, 251 Bayview Boulevard, Baltimore, MD 21224

[2]Department of Chemistry and Chemical Biology, Rutgers, The State University of New Jersey, 610 Taylor Road, Piscataway, NJ 08854

[3]Rutgers Cancer Institute of New Jersey, 195 Little Albany Street, New Brunswick, NJ 08901

Abstract

Repetitive DNA sequences, such as are present in micro- and mini-satellites, telomeres, and trinucleotide repeats (linked to fragile X syndrome, Huntington disease, etc.), account for nearly 30% of the human genome. These domains exhibit enhanced susceptibility to oxidative attack to yield base modifications, strand breaks and abasic sites, have a propensity to adopt non-canonical DNA forms modulated by the position(s) of the lesion(s), and, when not properly processed, can contribute to genome instability that underlies aging and disease development. Knowledge of the repair efficiencies of DNA damage within such repetitive sequences is therefore crucial for understanding the impact of such domains on genomic integrity. In the present study, using strategically designed oligonucleotide substrates, we determined the ability of human apurinic/apyrimidinic endonuclease 1 (APE1) to cleave at AP sites in a collection of tandem DNA repeat landscapes involving telomeric and CAG/CTG repeat sequences. Our studies reveal the differential influence of domain sequence, conformation, and AP site location/relative positioning on the efficiency of APE1 binding and strand incision. Intriguingly, our data demonstrate that APE1 endonuclease efficiency correlates with the thermodynamic stability of the DNA substrate. We discuss how these results have both predictive and mechanistic consequences for understanding the success and failure of repair protein activity associated with such oxidatively sensitive, conformationally plastic/dynamic repetitive DNA domains.

Keywords

APEX1; AP or abasic site; tandem repeat; telomere; trinucleotide expansion

[#]corresponding author: wilsonda@mail.nih.gov, (410) 558 8153.
[*]current address: Cancer Center, Daping Hospital, Third Military Medical University, No. 10 Changjiang Zhi Rd., Yuzhong Dist., Chongqing, China 400042

INTRODUCTION

Abasic sites, also known as apurinic/apyrimidinic (AP) sites, are one of the most common forms of DNA damage, with an estimated occurrence of ~10,000 per mammalian genome per day ([1]). Abasic sites entail the loss of the base moiety from the intact sugar phosphate backbone and are generated by spontaneous hydrolysis or from base lesion removal by DNA glycosylases. If unrepaired, since the genetic information carried by the original base residue is missing, AP sites can lead to error-prone bypass synthesis and thus cause mutagenesis (reviewed in ([2])). Moreover, the presence of an abasic lesion on a DNA template can impede the progression of a polymerase during replication or transcription ([3-6]), leading to genomic instability or gene expression defects, respectively.

Due to the high occurrence of abasic sites in the human genome and their potential to cause deleterious biological outcomes, investigators have worked to delineate the repair mechanisms for such damages. Class II AP endonucleases are the predominant AP site processing activity in most organisms and incise the phosphodiester backbone immediately 5′ to the lesion, generating a single-strand break with 3′-hydroxyl and 5′-deoxyribose phosphate (dRp) termini ([7]). Subsequent enzymes of the base excision repair (BER) pathway remove the 5′-dRp group, fill the gap, and seal the remaining nick to complete AP site repair ([8, 9]). In mammals, the major AP endonuclease is APE1, a protein that accounts for >95% of the total abasic site incision activity in human cell extracts (reviewed in ([10])).

Although it is thought that much of the human genome adopts canonical B-form right-handed double helical structure, many alternative DNA conformations are known to exist, and their roles in affecting biological processes have just begun to be understood (reviewed in ([11])). In particular, repetitive DNA sequences, which account for nearly 30% of the human genome, frequently are able to adopt a range of non-canonical DNA forms (i.e., non-B), in addition to the conventional duplex configuration. These sequences, which are often found in biologically interesting regions of the genome, also have a tendency to contribute to genome instability. Tandem DNA repeats are a subcategory of repetitive DNA, consisting of at least two nucleotides directly adjacent to each other in repetition, such as seen in microsatellites (1-7 nt) or minisatellites (10-100 nt). Prototypes for tandem DNA repeats include telomeric DNA and trinucleotide repeats (TNRs), genomic regions known to play critical roles in aging and disease development, such as in inherited neurological and neuromuscular disorders, including fragile X syndrome, Huntington disease, and myotonic dystrophy ([12, 13]).

Emerging evidence indicates that certain domains of the genome, including highly repetitive DNA sequences, are more susceptible to oxidative attack. For example, GGG-rich sequences, which are found in telomeric repeats (TTAGGG), centromeres and some putative gene control regions, are preferential targets of reactive oxygen species (ROS) generated by normal oxidative phosphorylation or as a result of an exposure or pathological condition that induces oxidative stress (reviewed in ([14])). In addition, Jarem et al. found that oxidative base lesions are preferentially generated by peroxynitrite within the loop domains of CAG repeat-containing DNA molecules, such as found in Huntington disease, in comparison to the normal duplex region ([15]). Yet, while scientists are gaining a better appreciation for the

susceptibility of certain genomic domains to DNA modification, we have only a cursory understanding of the molecular consequences of such damage or how it is repaired.

Previous studies have demonstrated that several elements can influence the AP endonuclease efficiency of APE1, including nearby damage, the overall nucleic acid conformational state, and the nucleotide sequence context (see for example, ([16-21])). In particular, in addition to cleaving at AP sites in normal duplex DNA, APE1 can incise at abasic sites in (1) single-stranded DNA, (2) certain bubble contexts, (3) the DNA strand of a DNA/RNA hybrid, and (4) single-stranded RNA. APE1 can also cleave at AP sites in "pseudo-triplex" bubble substrates designed to mimic a stalled replication or transcription intermediate and configurations that recapitulate an R-loop structure that exists during class switch recombination. In the present study, we determined the ability of APE1 to cleave at abasic sites in a collection of tandem DNA repeat landscapes involving telomeric and CAG/CTG sequences. Our investigations indicate an effect of the location of an AP site on the efficiency of APE1 incision and reveal an empirical correlation between the impact on duplex stability of the substrate AP lesion and the proximal domains on the modulation of repair protein activity, an observation foreshadowed by our previous studies ([22, 23]). Such data indicate that DNA damage will be repaired or processed with different proficiency, and thus, that certain genomic regions/domains will be more prone to damage accumulation and mutagenesis.

RESULTS

APE1 cleaves at AP sites in the double-stranded telomere domain, but not the single-stranded region

Given that telomere repeats are susceptible to oxidative modification and that APE1 deficiency leads to pronounced telomere defects ([14, 24]), initial experiments determined the ability of purified recombinant human APE1 protein to incise at a single abasic site within a telomeric context using a series of synthetic oligomers (Fig. 1A). Two telomeric repeat sequences (i.e., TTAGGG) were positioned within the middle of a 39-bp duplex to mimic the double-stranded region of a telomere ([25]), with guanine being replaced by the abasic site analog tetrahydrofuran (THF or F) where indicated. The control substrate (NTC39) possesses a similar base content, but with a randomly organized central sequence. As shown in Fig 1B, APE1 incises the abasic site at each of the three guanine positions within the first telomeric repeat unit efficiently (AP-1 substrates), although there exists a statistically significant ~2-fold variability in specific activity based on the precise lesion location (Fig. 1C, black bars; summarized in Table 1). We also measured the incision activity of APE1 at an abasic site near the double-stranded/single-stranded telomeric junction (OH57-DS), and in the 3′-single-stranded overhang (OH57-SS). These studies reveal that APE1 efficiently cuts at an AP site in the double-stranded portion of the telomeric substrate, but not within the single-stranded tail (Fig. 1B and C, black bars).

The pattern of AP site incision in telomere sequences by HeLa cell extract mimics that of purified APE1

We next compared the incision activity of purified recombinant APE1 to that of a whole cell extract (WCE) prepared from the HeLa cervical cancer cell line using the same series of control and telomeric AP-DNA substrates. We point out that as the abasic site analogue THF is resistant to AP lyase cleavage, the observed incision activity is limited to class II AP endonuclease processing ([26]). Strikingly, we found that purified APE1 and the HeLa extract exhibited essentially identical incision profiles for the various abasic site-containing telomeric DNAs (Fig. 1B and 1C, textile bars), although the WCE displayed an ~1.6-fold higher relative efficiency on OH57-DS as compared to the purified protein.

Western blotting was used to quantify the amount of APE1 in the HeLa WCE (Fig. 1D) and revealed that there is roughly 1.6 ± 0.02 pg of APE1 per ng of total extract. Extrapolating the available information, and assuming that APE1 is the major if not sole AP site incision activity in human cells ([27]) and data herein), indicates that the specific activity of the APE1 enzyme in a WCE context is 42 ± 13 pmol·min^{-1}·μg^{-1} for the NTC39 substrate. Comparing this value with the specific activity of purified APE1 against NTC39, which is 265 ± 65 pmol·min^{-1}·μg^{-1} (Table 1), indicates an ~6-fold inhibition in extracts that presumably reflects endogenous protein interference (i.e., DNA substrate binding or protein-protein interactions), the presence of inhibitory ligands in the WCE, or post-translational modification of APE1.

APE1 cleavage at clustered abasic sites in telomeric repeats is dependent on lesion arrangement

To further investigate APE1 incision at abasic sites in telomeric repeats, which as noted earlier are prone to oxidative modification and presumably clustered damage, we employed oligonucleotide substrates that contained at least two lesions (Fig. 2A) and were variations of the single AP site-containing substrates described above (compared in Table 1). Since APE1 activity could generate multiple products by cleavage at the different lesion sites, we used both 5′-end and 3′-end labeled substrates for these experiments. In addition, all reactions were separated on high-resolution denaturing sequencing gels to clearly distinguish the single base products possible for the AP-3 substrate. As seen above, purified recombinant APE1 and HeLa WCE showed a similar incision pattern for all substrates (Fig. 2B). Moreover, regardless of the location of the ^{32}P label, cleavage of AP-2a and AP-2b generated two products, whereas AP-3 reactions revealed only a single product. Based on mobility and signal intensity, APE1 appears to incise the upstream abasic site with greater efficiency in AP-2a and AP-2b (Fig. 2C), while the upstream-most lesion in the clustered abasic site set of AP-3 is seemingly the only damage processed by the enzyme. Interestingly, in vitro analyses have indicated that the 5′ most guanine of a GGG tract displays the greatest susceptibility to oxidative modification ([28]) and references therein).

AP sites within a CAG repeat duplex are recognized and processed by APE1, whereas those in a CAG repeat bulge loop are not

Previous work found that an abasic site in the duplex or loop domain of a CAG repeat “bulge loop” DNA substrate can differentially affect the stability of the loop structure,

implying that the lesion, and its position within the repeat, may play a role in TNR expansion ([22, 29]), a phenomenon common to inherited neurological disorders such as Huntington disease. We have extended these prior studies by examining whether the various AP site-containing CAG substrates affect processing by the human APE1 protein. In particular, a set of $(CAG)_6$ repeat-containing oligonucleotides harboring a single abasic site were annealed to either a 22-nt strand without the complimentary CTG repeats to form bulge loop ("BL") constructs or a 40-nt fully complimentary strand with six CTG repeats to form the corresponding ("40") duplex constructs (Fig. 3A). The parent 22 mer duplex substrate (22 mer) without the CAG/CTG repeats was included as a comparative control. In all of these DNAs, the abasic site, regardless of location, is surrounded by the same nearest neighbor bases (A**F**C) and, in the case of the double-stranded molecules, is always opposite a C. Thus, it is the surrounding sequence domain and/or the nature of the DNA secondary structure that changes and will be responsible for any observed variation in APE1 activity.

Our studies found that the abasic sites within the $(CAG)_6$ bulge loop are generally resistant to APE1 incision (BL6-F1, BL6-F3 and BL6-F5), whereas the same abasic sites in the fully annealed 40 mer duplex substrates (40-F1, 40-F3 and 40-F5) were cleaved effectively (Fig. 3B). However, it is worth pointing out that the abasic site in the 5′ portion of the loop domain (BL6-F1) was cleaved with some small efficiency relative to the other bulge loop substrates (summarized in Table 1). When the abasic site was positioned within the duplex domain upstream of the $(CAG)_6$ loop (BL6-FStem), APE1 was able to process the lesion competently. These observations were supported by both time- and dose-dependent incision assays (Fig. 3C and 3D). When comparing the specific activities of APE1 for the different substrates with an AP site in a double-stranded region, i.e., BL6-FStem, 40-FStem, 40-F1, 40-F3 and 40-F5, the latter three DNAs, which harbor the AP site within the CAG repeats, were processed ~2 to 3-fold less effectively (Table 1). Moreover, the incision efficiency of APE1 for the BL6-FStem and 40-FStem substrates was ~3 to 4-fold lower than for the control 22 mer substrate (Table 1), even though the non-repetitive DNA sequence immediately surrounding the AP site (i.e., the five bases upstream and downstream) is the same in all three constructs. Cumulatively, these data indicate a broad, adverse effect of TNRs on enzyme processing. Finally, consistent with the data above using the telomeric substrates, the same pattern of AP site incision activity was observed for the CAG repeat-containing substrates with either purified APE1 or HeLa WCE (Fig. S1).

Lack of AP site incision of bulge loop constructs is due to a defect in APE1 DNA binding

We next determined if the ability of APE1 to incise at the abasic site was related to binding efficiency of the protein using a previously established electrophoretic mobility shift assay (EMSA) ([30]). As evident from the data presented in Fig. 4A and B, the observed APE1-DNA complex was more or less absent for the bulge loop substrates as compared to substrates harboring an AP site within duplex DNA ($p<0.01$), implying that recognition and binding is greatly diminished for damage in the loop domain.

Variation in APE1 incision on CAG duplex substrates is primarily due to reduced catalytic efficiency

Since the EMSA data indicated an affinity for the 40-F1, 40-F3 and 40-F5 CAG substrates that is comparable to the 22 mer (Fig. 4B), despite the ~10-fold lower incision activity of the protein for the 40 mer duplexes (Table 1), we determined more quantitatively the ability of APE1 to form a stable complex with either the 22 mer or 40-F3 (as a representative substrate) using protein titration experiments. As shown in Fig. 4C, the apparent binding affinities for the 22 mer and 40-F3 DNAs are indeed surprisingly similar, with 50% substrate bound at approximately 15 ng and 26 ng APE1, respectively. We also determined the steady-state kinetic parameters for APE1 incision of the 22 mer and 40-F3 substrates: K_m values were 55 and 23 nM; V_{max} values were 8.3 and 0.93 nM min^{-1}; and k_{cat} values were 5.9 and 0.66 min^{-1}, respectively. These data suggest that the inability of APE1 to efficiently incise at AP sites in the $(CAG)_6$ repeat tract stems largely from a catalytic impediment and is not due to “titrating-off” of the enzyme via nonspecific binding to the excess DNA in the longer 40 mer duplexes.

Neighboring bulge loops have varying effects on APE1 incision activity in adjacent duplex domains

We next examined the influence of the size and location of a bulge loop on the ability of APE1 to cleave at an AP site within a nearby duplex using a set of TNR-containing DNA substrates (Fig. 5A). As seen in Fig. 5B, a DNA substrate harboring a $(CAG)_8$ bulge loop on the same strand as an upstream AP site (BL8-FStem) was incised ~2-fold more efficiently (in the linear range of enzymatic activity, i.e, at 5 min) than a comparable substrate with a $(CAG)_6$ loop (BL6-FStem). When the loop was positioned on the strand opposite the AP site, there was a consistent trend for APE1 incision to be stimulated relative to the normal duplex (22 mer = CAG0F:CTG0), particularly with the $(CTG)_2$ loop size (Fig. 5C, black bars). If the abasic lesion was on the CTG strand within the neighboring duplex, APE1 exhibited a similar incision efficiency regardless of the strand opposite CAG loop size (Fig. 5C, grey bars), although the complex with a $(CAG)_2$ loop appeared to be cleaved at a slightly diminished capacity. One noteworthy observation is that the substrates harboring the AP site in the CTG strand (CTG0F) were cleaved at roughly half the initial rate of the CAG abasic substrates (CAG0F; Fig. 5C and summarized in Table 1). This outcome may reflect a steric hindrance to enzyme binding due to the nearby loop or the reduced thermodynamic stability of the CAGN:CTG0F constructs that likely introduces partially denatured states under the conditions of the experiment.

Impact on APE1 incision of dynamic complementarity in AP site-containing TNR bulge loop

TNRs are dynamic in nature, taking on a range of conformational states that are influenced by the sequence context and location of DNA damage ([29]). We examined here the effect of the presence of a $(CTG)_2$ stretch opposite the various AP site-containing bulge loop substrates tested above (see Fig. 3A and 6A) on APE1 incision activity. We showed previously for a CAG8 oligomer annealed to a “CTGN” strand (N = 2, 4, 6), that the repeat bulge loop can exist in multiple isoenergentic structural arrangements, with relatively facile

inter-conversion between them, prompting the designation “rollamers” ([31]). The relative population of loop isomers is influenced by the relative thermodynamic impact of the abasic site and its position within the repeat, with the lesion favoring isomer states that are least energetically perturbed. CAG6F1, CAG6F3, and CAG6F5 annealed to CTG2 result in the formation of loop isomers that differ structurally in that the abasic site can be located in different structural elements of the overall bulge loop construct: i.e., in the upstream duplex (CAG6F1), the 5′ duplex loop junction (CAG6F1), the loop (CAG6F1, CAG6F3, CAG6F5), the 3′ duplex loop junction (CAG6F5), or the downstream duplex domain (CAG6F5) ([31]).

In the experiments here, we found that APE1 (500 pg) was able to efficiently incise only the CAG6F1:CTG2 substrate (Fig. 6B), where the abasic site is located in the 5′ region of the CAG domain and can partition into the upstream duplex, the 5′ duplex loop junction, or the loop domain. When APE1 protein was increased to 25 ng, we did observe cleavage of all three substrates to varying degrees (Fig. S2; Table 1). An EMSA revealed that APE1 binds most stably to CAG6F1:CTG2, which it cleaves, whereas APE1 does not appear to bind significantly to the poorly incised CAG6F3:CTG2 and CAG6F5:CTG2 substrates (Fig. 6C). In other words, substrates that cannot be processed efficiently are also not bound stably, similar to what we observed with static CAG repeat bulge loops earlier.

APE1 binds only one of the rollamer isoforms that can be resolved electrophoretically

The EMSA revealed (at least) two prominent labeled DNA species of differing migration for the CAG6F1:CTG2 and CAG6F5:CTG2 substrates in the native gel (Fig. 6C), likely reflecting the different conformational states that can be adopted by these rollamers. Although CAG6Fn:CTG2 can form three distinct loop isomers “on paper”, it is likely that only two are resolvable on a gel, as two of the loop isomers (i.e., the one with a long upstream and short downstream arm, and the one with a long downstream and short upstream arm) are expected to have very similar hydrodynamic properties. The fact that we observed only one major species for CAG6F3:CTG2 suggests that for this oligomer arrangement the different loop isomers are not resolvable, or more likely, that only one of the isomers is populated to a significant extent ([32]).

The impact of partitioning of the abasic site into different structural elements of the bulge loop constructs is also reflected in the temperature induced strand dissociation behavior of these constructs, where the CAG6F1:CTG2 substrate recognized/processed by APE1 exhibits a unique denaturation curve relative to CAG6F3:CTG2 and CAG6F5:CTG2 (Fig. 6D). The altered shape of the curve (green trace) reflects changes in the dissociation pathway induced by the 5′ location of the abasic site and the associated variation in rollamer distribution/dissociation pathway caused by destabilization of the upstream domain. Interestingly, APE1 appears to only bind the slower migrating species of the CAG6F1:CTG2 substrate in the EMSA (Fig. 6C), albeit with low affinity as suggested by the observed smear, indicating that the enzyme may preferentially associate with one particular structural form. Based on our incision results described earlier, this DNA species is likely to be the rollamer isomer where the abasic site is partitioned into the upstream duplex domain (similar to BL6-FStem). Collectively, the results within support the

conclusion that APE1 is able to recognize and process lesions on the 5′ side of a bulge loop, albeit with reduced affinity, whereas the enzyme is unable to process lesions within the 3′ portion of the bulge loop and 3′ of a nearby bulge loop. Future work will need to determine how APE1 binding and/or processing of the AP site influences the repeat bulge loop distribution in the rollamer substrates.

DISCUSSION

Tandem repeats, such as those found in telomeres (e.g., TTAGGG) or in TNR disorders (e.g., CAG), display increased susceptibility to oxidative modification and can exhibit enhanced instability that contributes to aging and disease etiology. Studies are at the early stages of delineating how repetitive DNA and non-canonical DNA conformations can affect various DNA metabolic processes, such as DNA repair. Using a series of synthetic oligonucleotide substrates, we determined the ability of APE1 to recognize and process abasic sites in two prototypical tandem repeat settings: telomeric and trinucleotide repeats. The observation that APE1 processes AP sites with varying efficiency, depending on sequence and context (Table 1), has important implications in terms of DNA damage persistence within and mutagenic potential of different genomic domains.

Repair of oxidative damage in TNR sequences affects expansion/contraction events

McMurray and colleagues reported that oxidative damage in CAG repeat tracts can drive expansion, such as seen in Huntington disease, through an OGG1 DNA glycosylase-initiated BER response ([33]). Subsequent work demonstrated that the DNA glycosylase NEIL1 can also promote TNR instability ([34]). Our investigations here indicate that APE1 poorly operates on AP sites within a looped-out domain of a TNR substrate, generally consistent with our prior finding ([35]). Moreover, AP sites within a double-stranded CAG stretch (40-F1, -F2, and -F3) are significantly poorer substrates for APE1 than when located in a more random nucleotide sequence (e.g., the 22 mer). Furthermore, experimental studies indicate that single-stranded loops are more susceptible to oxidative modification (see for instance, ([15])), and thermodynamic arguments suggest that lesions will favor partitioning of the damage into the bulge loop structure ([29]). These facts, collectively, contend that genomic regions susceptible to looped-out structures, such as TNR tracts, will be prone to damage accumulation and a poor repair outcome.

When APE1 incision does take place within a TNR stretch, presumably in a duplex portion, BER can promote instability in a manner that is influenced by (i) the location of the lesion within the repeat array (i.e., 5′ or 3′) and (ii) the stoichiometry of the BER protein concentrations ([35-40]). Based on the observation that APE1 incises at AP sites with some low level activity only when in the 5′ loop position of the rollamer substrate, it is tempting to speculate that this cleavage event would lead to the formation of a gap immediately upstream of a stable repeat fold-back self-structure (often inaccurately referred to as a “5′-hairpin”), an outcome that would in turn lead to TNR expansion via repair synthesis and ligation.

It is noteworthy that APE1 binding to an AP site within a $(CAG)_6$ double-stranded array is not dramatically affected, whereas the catalytic efficiency is markedly reduced (nearly 10-

fold). Such a finding suggests that while APE1 is able to form a stable complex with an AP site within a TNR sequence tract, it is unable to establish the transition state intermediate required for metal-assisted strand scission. It is possible that this binding serves as a protective strategy for an AP site intermediate in such a genomic domain or helps to coordinate the BER response in a “passing-the-baton”-type mechanism. However, persistent DNA damage could eventually lead to mutagenic events or reduced transcriptional efficiency.

Repair of abasic sites by APE1 in telomeres is important for telomere function

Evidence has begun to emerge that reveals a particularly important role for BER in the maintenance of telomeric integrity and functionality, which likely has significant implications for aging and disease development ([41-46]). In the case of APE1, a recent study demonstrated that depletion of the protein causes telomere dysfunction, including telomere signal loss, chromosome end fragmentation, chromosome end-to-end fusions, and extra telomeric signals ([24]). We found that APE1 efficiently incises at a single abasic site in a simple telomeric repeat, but that the protein poorly processes lesions in certain clustered arrangements. The enzyme is especially sensitive to neighboring 5′ modifications, such as a nearby AP site (see also ([17, 20])), particularly when located within the region that APE1 makes its most intimate contacts with DNA ([47]). Modifications 3′ to an abasic lesion have a less noticeable effect on APE1 incision capacity, and in the case of a 3′ mismatch have even been found to be stimulatory ([16]). We speculate that the propensity of telomeric DNA to sustain oxidative modification likely gives rise to clustered lesions that would be either poorly processed or converted into double-strand breaks by BER ([48]), culminating in telomeric defects. Moreover, damage persistence or accumulation within the telomeric region would likely result in defective binding of TRF1 and TRF2 to telomeric repeats ([49]), two proteins that are part of the protective shelterin complex, further promoting telomere instability.

We found herein that APE1 exhibits poor incision at an AP site within the single-stranded portion of a model telomeric substrate. However, the issue of APE1 activity on single-stranded DNA is complex, as prior studies have revealed efficient cleavage of single-stranded substrates by the human enzyme ([50]). One confounding factor is that “single-stranded” DNA often takes on some form of self-structure, typically due to intramolecular folding. Our prior work demonstrated that APE1 has a >100-fold lower incision efficiency on poly(dA) or poly(dT) oligonucleotides harboring a single AP site relative to their comparable double-stranded substrates ([51]), suggesting that mostly single-stranded molecules are poorly processed by the repair protein. More extensive analyses, which included a wide-range of oligonucleotides, support the conclusion that fortuitous secondary structure is a key element in dictating APE1 cleavage efficiency of so-called single-stranded molecules ([51]).

APE1 DNA repair activity is influenced by sequence context and thermodynamic stability

Another notable element of the studies herein is the observation that APE1 cleavage efficiency for a family of closely-related 40 mer duplexes containing the same lesion in the same sequence/nearest neighbor context correlates with their thermodynamic stability. As

shown in more detail in Figure 7, within the uncertainty of the experimental data, there is a striking similarity in the pattern of APE1 incision with lesion position (panel A) or loop size (panel B) and the thermodynamic stability of these constructs. However, this correlation is less obvious when comparing across different DNA constructs (e.g., 22 mer, BL-FStem, 40FStem), probably because the local and global thermodynamic impact of the lesion is distributed differently in these variable substrates. Nevertheless, the general trend seems to persist and is noteworthy. The observed position-dependent variation in AP site energetics for the above sequence-controlled 40 mer constructs suggests coupling between the lesion and the oligomer ends, with there being a more pronounced effect the closer the lesion is to the end. Consistently, we previously had shown energetic coupling between abasic sites and nearby bulge loop structures ([22, 23]).

Interestingly, a similar correlation between thermodynamic stability of lesion-containing DNA duplexes and either repair glycosylases or *Escherichia coli* endonuclesse IV has been reported ([52-56]). It was argued that the correlation between thermodynamic stability and enzyme activity for DNA glycosylases reflects the enzymatic recognition/binding process, which requires ‘flipping out’ of the substrate base from the helical stack. Structural insights from X-ray crystal data of APE1 with and without duplex substrates indicate that the protein binding pocket remains relatively unperturbed, whereas the DNA substrate undergoes a substantial structural rearrangement upon protein binding ([47]). It is therefore tempting to interpret the observed correlation between lesion thermodynamics and enzyme efficiency as a component of substrate flexibility that involves damage recognition and/or transition state competency. Our experimental data, albeit limited, indicate that the variation in APE1 activity is primarily due to changes in k_{cat} and not K_M, implying that, unlike for uracil DNA glycosylase, it is not energetic lesion recognition, but transition state formation or product release (i.e., the reaction chemistry) that is responsible for the observed repair efficiency-thermodynamic stability correlation seen for APE1. These preliminary conclusions will of course need to be interrogated in greater detail by more quantitative studies in the future. Regardless of the origins of the observed thermodynamic-function relationship, the finding that APE1 can process AP sites with varying degrees of efficiency depending on the nucleotide context suggests that lesions will exhibit variable consequences on the nature and effectiveness of the repair response, and ultimately, on the integrity of the genome. It will be particularly interesting to examine how such features might affect possible genome-specific coordination of the BER response.

APE1 appears to be the major factor in recognition and processing of AP site lesions within non-canonical DNA secondary structures

APE1 is the major AP endonuclease in human cells, is a robust enzyme, and is present at generally high concentrations ([10, 27]). However, it was still surprising to us that the incision profile for the HeLa WCE was essentially identical to that obtained with the purified recombinant protein, with the single major difference being the estimated ~6-fold inhibition of APE1 activity in the WCE context. We propose that the reduced incision efficiency of APE1 stems from other DNA binding proteins in the extract associating with the DNA substrate, direct protein interactions, and/or post-translational modification. In addition, the results suggest that the same pathways critical for the repair of abasic sites in “normal”

duplex DNA are important for the repair of lesions in non-canonical DNA secondary structures. In other words, no obvious DNA secondary structure-specific pathway exists for processing AP sites embedded within non-canonical DNA forms. Future studies will focus on delineating the factors that fine-tune the endonuclease efficiency of human APE1.

MATERIALS AND METHODS

Recombinant human APE1 protein and HeLa WCE

Untagged, human recombinant APE1 protein was overexpressed from pETApe and purified to >95% purity as essentially described ([57]). Exponentially growing HeLa cells were harvested by trypsinization and washed once with cold PBS. The cell pellet was then resuspended at a density of 10^7 cells/mL in Lysis Buffer (50 mM Tris HCl pH 7.4, 150 mM NaCl, 1 mM EDTA and 1% (vol/vol) Triton X-100 supplemented with 0.5 mM PMSF and protease inhibitor cocktail) and incubated for 30 min at 4°C. After centrifugation at 18,000 g for 20 min at 4°C, the supernatant was collected as the WCE. Protein concentrations were determined using the Bradford method.

Oligonucleotide substrates

Oligonucleotides were purchased from Integrated DNA Technologies (Coralville, IA) or synthesized as described ([29, 31]). Oligonucleotide names and sequences are listed in Table 2. For abasic site incision assays, oligonucleotides containing an abasic site analog (THF) were radiolabeled at either the 5′ end using [γ-^{32}P]ATP and T4 polynucleotide kinase (New England Biolabs, Ipswich, MA) or the 3′ end using [α-^{32}P]dCTP and terminal deoxynucleotidyl transferase (New England Biolabs, Ipswich, MA). Oligonucleotides were annealed by heating at 95 °C for 3 min and then cooling 2 °C every 2 min to 25 °C in a thermocycler. Annealing of the substrates was verified by native polyacrylamide electrophoresis.

AP site incision assay

All incision experiments were conducted under steady-state conditions and within the linear range of the assay. For telomeric substrates, the indicated amount of APE1 or WCE was incubated with radiolabeled THF-containing oligonucleotide substrates at 37 °C under physiologically relevant reaction conditions (50 mM HEPES-KOH pH 7.5, 50 mM KCl, 1 mM $MgCl_2$, 1 mM DTT). For TNR substrates, the indicated amount of APE1 or WCE was incubated with radiolabeled substrates at 25 °C under modified reaction conditions (10 mM HEPES-NaOH pH 7.5, 100 mM NaCl, 2 mM $MgCl_2$). Reactions were inhibited by the addition of stop buffer (95% formamide, 20 mM ETDA, 0.5% bromphenol blue, and 0.5% xylenecyanol), and then heated at 95 °C for 5 min. Reaction products were resolved by 15% polyacrylamide urea denaturing gel electrophoresis, imaged, and quantified using a Typhoon phosphoimager and ImageQuant TL software (GE Healthcare, Piscataway, NJ). Steady-state kinetic parameters were determined by incubating 500 pg (1.4 nM) of APE1 in 10 μl with 5, 10, 25, 50 or 100 nM 22 mer or 40-F3 substrate for 5 min at 25 °C. Reaction velocities were calculated following denaturing gel electrophoresis as described above. K_m and V_{max} were determined using Lineweaver-Burk plots in Prism 6 software (GraphPad Software, La Jolla, CA).

APE1 DNA binding assay

APE1-DNA complex formation was assessed essentially as described ([30]). Each reaction contained 100 fmol of DNA substrate (10 nM) and the indicated amount of APE1 protein in a final volume of 10 μl. The binding reactions were separated on an 8% native gel at 4 °C. The percentage of labeled DNA bound was determined by standard phosphorimager and ImageQuant TL software analysis (GE Healthcare, Piscataway, NJ).

Western blot analysis

Three μg HeLa WCE or the indicated amount of recombinant APE1 protein was mixed with 2× loading buffer (50 mM Tris pH 6.8, 2% SDS, 2% 2-mercaptoethanol, 12% glycerol) and heated at 95°C for 5 min before loading on a 10% SDS-polyacrylamide gel. After electrophoresis, proteins were transferred to a nitrocellulose membrane. In-house rabbit polyclonal APE1 antibody was used at a dilution of 1:10,000 to detect the protein, followed by an HRP-conjugated goat anti-rabbit secondary antibody. The membrane was washed using standard procedures, and the ECL substrate (GE Healthcare, Piscataway, NJ) was applied. The blot image was visualized by ChemiDoc XRS System and analyzed by Image Lab™ Software (Bio-Rad Laboratories, Hercules, CA).

Thermodynamic studies

Thermodynamic parameters for the DNA substrates were derived from model free differential scanning calorimetry studies conducted using a NanoDSCII (Calorimetry Science Corporation, Lindon, UT) with a nominal cell volume of 0.3 ml as described ([58-60]). Oligonucleotides, at a concentration of 50 μM per strand, were repeatedly scanned between 0 °C and 90 or 95 °C with a constant heating rate of 1 °C/min, while continuously recording the excess power required to maintain sample and reference cells at the same temperature. After conversion of the measured excess power values to heat capacity units and subtraction of buffer vs. buffer scans, the raw differential scanning calorimetry traces were normalized for DNA concentration and analyzed using Origin software (Originlabs Corp., Northampton, MA). The calorimetric enthalpy (ΔH_{cal}) was derived by integration of the excess heat capacity curve, and ΔC_p was derived from the difference in the linearly extrapolated pre- and post-transition baselines at T_m. ΔS was derived by $\Delta H/T_m$, assuming "pseudomonomolecular" behavior in which propagation dominates initiation in the strand dissociation mechanism ([61, 62]). The T_m is defined as the temperature at the midpoint of the integrated excess heat capacity curve for a given conformational transition, which corresponds to half the sample being denatured for a process that exhibits pseudomonomolecular behavior. The free energy change at a suitable reference temperature was derived from the well-known standard identity: $\Delta G(T) = \Delta H_{cal}(T_m - T)/T_m - \Delta C_p(T_m - T) + T\Delta C_p \ln(T_m/T)$.

Supplementary Material

Refer to Web version on PubMed Central for supplementary material.

Acknowledgments

We wish to thank Drs. Yie Liu (NIA) and Dr. G. Eric Plum (IBETinc., Columbus, OH) for their constructive comments on the manuscript. This research was supported by the Intramural Research Program at the NIH, National Institute on Aging; and NIH grants GM23509, GM34469 and CA47995 (to K.J.B.).

Abbreviations

AP	apurinic/apyrimidinic
APE1	AP endonuclease 1
BER	base excision repair
dRp	deoxyribose phosphate
EMSA	electrophoretic mobility shift assay
ROS	reactive oxygen species
THF or F	tetrahydrofuran
TNR	trinucleotide repeat
WCE	whole cell extract

Reference List

1. Lindahl T. Instability and decay of the primary structure of DNA. Nature. 1993; 362:709–715. [PubMed: 8469282]
2. Loeb LA, Preston BD. Mutagenesis by apurinic/apyrimidinic sites. Annu. Rev. Genet. 1986; 20:201–230. [PubMed: 3545059]
3. Shibutani S, Takeshita M, Grollman AP. Translesional synthesis on DNA templates containing a single abasic site. A mechanistic study of the “A rule”. J. Biol. Chem. 1997; 272:13916–13922. [PubMed: 9153253]
4. Mozzherin DJ, Shibutani S, Tan CK, Downey KM, Fisher PA. Proliferating cell nuclear antigen promotes DNA synthesis past template lesions by mammalian DNA polymerase delta. Proc. Natl. Acad. Sci. U. S. A. 1997; 94:6126–6131. [PubMed: 9177181]
5. Locatelli GA, Pospiech H, Tanguy Le GN, van LB, Hubscher U, Parkkinen S, Syvaoja JE, Villani G. Effect of 8-oxoguanine and abasic site DNA lesions on in vitro elongation by human DNA polymerase in the presence of replication protein A and proliferating-cell nuclear antigen. Biochem. J. 2010; 429:573–582. [PubMed: 20528769]
6. Tornaletti S, Maeda LS, Hanawalt PC. Transcription arrest at an abasic site in the transcribed strand of template DNA. Chem. Res. Toxicol. 2006; 19:1215–1220. [PubMed: 16978026]
7. Mosbaugh DW, Linn S. Further characterization of human fibroblast apurinic/apyrimidinic DNA endonucleases. The definition of two mechanistic classes of enzyme. J. Biol. Chem. 1980; 255:11743–11752. [PubMed: 6254980]
8. Kim YJ, Wilson DM III. Overview of base excision repair biochemistry. Curr. Mol. Pharmacol. 2012; 5:3–13. [PubMed: 22122461]
9. Dianov GL, Hubscher U. Mammalian base excision repair: the forgotten archangel. Nucleic Acids Res. 2013; 41:3483–3490. [PubMed: 23408852]
10. Li M, Wilson DM III. Human apurinic/apyrimidinic endonuclease 1. Antioxid. Redox. Signal. 2014; 20:678–707. [PubMed: 23834463]
11. Cooper DN, Bacolla A, Ferec C, Vasquez KM, Kehrer-Sawatzki H, Chen JM. On the sequence-directed nature of human gene mutation: the role of genomic architecture and the local DNA

sequence environment in mediating gene mutations underlying human inherited disease. Hum. Mutat. 2011; 32:1075–1099. [PubMed: 21853507]

12. Armanios M. Telomeres and age-related disease: how telomere biology informs clinical paradigms. J. Clin. Invest. 2013; 123:996–1002. [PubMed: 23454763]
13. Nelson DL, Orr HT, Warren ST. The unstable repeats--three evolving faces of neurological disease. Neuron. 2013; 77:825–843. [PubMed: 23473314]
14. von ZT. Oxidative stress shortens telomeres. Trends Biochem. Sci. 2002; 27:339–344. [PubMed: 12114022]
15. Jarem DA, Wilson NR, Delaney S. Structure-dependent DNA damage and repair in a trinucleotide repeat sequence. Biochemistry. 2009; 48:6655–6663. [PubMed: 19527055]
16. Wilson DM III, Takeshita M, Grollman AP, Demple B. Incision activity of human apurinic endonuclease (Ape) at abasic site analogs in DNA. J. Biol. Chem. 1995; 270:16002–16007. [PubMed: 7608159]
17. Chaudhry MA, Weinfeld M. Reactivity of human apurinic/apyrimidinic endonuclease and Escherichia coli exonuclease III with bistranded abasic sites in DNA. J. Biol. Chem. 1997; 272:15650–15655. [PubMed: 9188454]
18. Beloglazova NG, Kirpota OO, Starostin KV, Ishchenko AA, Yamkovoy VI, Zharkov DO, Douglas KT, Nevinsky GA. Thermodynamic, kinetic and structural basis for recognition and repair of abasic sites in DNA by apurinic/apyrimidinic endonuclease from human placenta. Nucleic Acids Res. 2004; 32:5134–5146. [PubMed: 15459284]
19. Wilson DM III. Ape1 abasic endonuclease activity is regulated by magnesium and potassium concentrations and is robust on alternative DNA structures. J. Mol. Biol. 2005; 345:1003–1014. [PubMed: 15644200]
20. Paap B, Wilson DM III, Sutherland BM. Human abasic endonuclease action on multilesion abasic clusters: implications for radiation-induced biological damage. Nucleic Acids Res. 2008; 36:2717–2727. [PubMed: 18353858]
21. Berquist BR, McNeill DR, Wilson DM III. Characterization of abasic endonuclease activity of human Ape1 on alternative substrates, as well as effects of ATP and sequence context on AP site incision. J. Mol. Biol. 2008; 379:17–27. [PubMed: 18439621]
22. Volker J, Plum GE, Klump HH, Breslauer KJ. Energetic coupling between clustered lesions modulated by intervening triplet repeat bulge loops: allosteric implications for DNA repair and triplet repeat expansion. Biopolymers. 2010; 93:355–369. [PubMed: 19890964]
23. Volker J, Plum GE, Klump HH, Breslauer KJ. Energy crosstalk between DNA lesions: implications for allosteric coupling of DNA repair and triplet repeat expansion pathways. J. Am. Chem. Soc. 2010; 132:4095–4097. [PubMed: 20218680]
24. Madlener S, Strobel T, Vose S, Saydam O, Price BD, Demple B, Saydam N. Essential role for mammalian apurinic/apyrimidinic (AP) endonuclease Ape1/Ref-1 in telomere maintenance. Proc. Natl. Acad. Sci. U. S. A. 2013; 110:17844–17849. [PubMed: 24127576]
25. Rhee DB, Ghosh A, Lu J, Bohr VA, Liu Y. Factors that influence telomeric oxidative base damage and repair by DNA glycosylase OGG1. DNA Repair (Amst). 2011; 10:34–44. [PubMed: 20951653]
26. Takeshita M, Chang CN, Johnson F, Will S, Grollman AP. Oligodeoxynucleotides containing synthetic abasic sites. Model substrates for DNA polymerases and apurinic/apyrimidinic endonucleases. J. Biol. Chem. 1987; 262:10171–10179. [PubMed: 2440861]
27. Demple B, Sung JS. Molecular and biological roles of Ape1 protein in mammalian base excision repair. DNA Repair (Amst). 2005; 4:1442–1449. [PubMed: 16199212]
28. Kawanishi S, Oikawa S. Mechanism of telomere shortening by oxidative stress. Ann. N. Y. Acad. Sci. 2004; 1019:278–284. [PubMed: 15247029]
29. Volker J, Plum GE, Klump HH, Breslauer KJ. DNA repair and DNA triplet repeat expansion: the impact of abasic lesions on triplet repeat DNA energetics. J. Am. Chem. Soc. 2009; 131:9354–9360. [PubMed: 19566100]
30. Wilson DM III, Takeshita M, Demple B. Abasic site binding by the human apurinic endonuclease, Ape, and determination of the DNA contact sites. Nucleic Acids Res. 1997; 25:933–939. [PubMed: 9023101]

31. Volker J, Gindikin V, Klump HH, Plum GE, Breslauer KJ. Energy landscapes of dynamic ensembles of rolling triplet repeat bulge loops: implications for DNA expansion associated with disease states. J. Am. Chem. Soc. 2012; 134:6033–6044. [PubMed: 22397401]
32. Volle CB, Jarem DA, Delaney S. Trinucleotide repeat DNA alters structure to minimize the thermodynamic impact of 8-oxo-7,8-dihydroguanine. Biochemistry. 2012; 51:52–62. [PubMed: 22148399]
33. Kovtun IV, Liu Y, Bjoras M, Klungland A, Wilson SH, McMurray CT. OGG1 initiates age-dependent CAG trinucleotide expansion in somatic cells. Nature. 2007; 447:447–452. [PubMed: 17450122]
34. Mollersen L, Rowe AD, Illuzzi JL, Hildrestrand GA, Gerhold KJ, Tveteras L, Bjolgerud A, Wilson DM III, Bjoras M, Klungland A. Neil1 is a genetic modifier of somatic and germline CAG trinucleotide repeat instability in R6/1 mice. Hum. Mol. Genet. 2012; 21:4939–4947. [PubMed: 22914735]
35. Goula AV, Berquist BR, Wilson DM III, Wheeler VC, Trottier Y, Merienne K. Stoichiometry of base excision repair proteins correlates with increased somatic CAG instability in striatum over cerebellum in Huntington's disease transgenic mice. PLoS. Genet. 2009; 5:e1000749. [PubMed: 19997493]
36. Liu Y, Prasad R, Beard WA, Hou EW, Horton JK, McMurray CT, Wilson SH. Coordination between polymerase beta and FEN1 can modulate CAG repeat expansion. J. Biol. Chem. 2009; 284:28352–28366. [PubMed: 19674974]
37. Goula AV, Pearson CE, Della MJ, Trottier Y, Tomkinson AE, Wilson DM III, Merienne K. The Nucleotide Sequence, DNA Damage Location, and Protein Stoichiometry Influence the Base Excision Repair Outcome at CAG/CTG Repeats. Biochemistry. 2012; 51:3919–3932. [PubMed: 22497302]
38. Derevyanko AG, Endutkin AV, Ishchenko AA, Saparbaev MK, Zharkov DO. Initiation of 8-oxoguanine base excision repair within trinucleotide tandem repeats. Biochemistry (Mosc.). 2012; 77:270–279. [PubMed: 22803944]
39. Lai Y, Xu M, Zhang Z, Liu Y. Instability of CTG repeats is governed by the position of a DNA base lesion through base excision repair. PLoS. One. 2013; 8:e56960. [PubMed: 23468897]
40. Jarem DA, Wilson NR, Schermerhorn KM, Delaney S. Incidence and persistence of 8-oxo-7,8-dihydroguanine within a hairpin intermediate exacerbates a toxic oxidation cycle associated with trinucleotide repeat expansion. DNA Repair (Amst). 2011; 10:887–896. [PubMed: 21727036]
41. Fotiadou P, Henegariu O, Sweasy JB. DNA polymerase beta interacts with TRF2 and induces telomere dysfunction in a murine mammary cell line. Cancer Res. 2004; 64:3830–3837. [PubMed: 15172990]
42. Muftuoglu M, Wong HK, Imam SZ, Wilson DM III, Bohr VA, Opresko PL. Telomere repeat binding factor 2 interacts with base excision repair proteins and stimulates DNA synthesis by DNA polymerase beta. Cancer Res. 2006; 66:113–124. [PubMed: 16397223]
43. Wang Z, Rhee DB, Lu J, Bohr CT, Zhou F, Vallabhaneni H, de Souza-Pinto NC, Liu Y. Characterization of oxidative guanine damage and repair in mammalian telomeres. PLoS. Genet. 2010; 6:e1000951. [PubMed: 20485567]
44. Miller AS, Balakrishnan L, Buncher NA, Opresko PL, Bambara RA. Telomere proteins POT1, TRF1 and TRF2 augment long-patch base excision repair in vitro. Cell Cycle. 2012; 11:998–1007. [PubMed: 22336916]
45. Vallabhaneni H, O'Callaghan N, Sidorova J, Liu Y. Defective repair of oxidative base lesions by the DNA glycosylase Nth1 associates with multiple telomere defects. PLoS. Genet. 2013; 9:e1003639. [PubMed: 23874233]
46. Zhou J, Liu M, Fleming AM, Burrows CJ, Wallace SS. Neil3 and NEIL1 DNA glycosylases remove oxidative damages from quadruplex DNA and exhibit preferences for lesions in the telomeric sequence context. J. Biol. Chem. 2013; 288:27263–27272. [PubMed: 23926102]
47. Mol CD, Izumi T, Mitra S, Tainer JA. DNA-bound structures and mutants reveal abasic DNA binding by APE1 and DNA repair coordination. Nature. 2000; 403:451–456. [PubMed: 10667800]
48. Georgakilas AG, O'Neill P, Stewart RD. Induction and repair of clustered DNA lesions: what do we know so far? Radiat. Res. 2013; 180:100–109. [PubMed: 23682596]

49. Opresko PL, Fan J, Danzy S, Wilson DM III, Bohr VA. Oxidative damage in telomeric DNA disrupts recognition by TRF1 and TRF2. Nucleic Acids Res. 2005; 33:1230–1239. [PubMed: 15731343]
50. Marenstein DR, Wilson DM III, Teebor GW. Human AP endonuclease (APE1) demonstrates endonucleolytic activity against AP sites in single-stranded DNA. DNA Repair (Amst). 2004; 3:527–533. [PubMed: 15084314]
51. Fan J, Matsumoto Y, Wilson DM III. Nucleotide sequence and DNA secondary structure, as well as replication protein A, modulate the single-stranded abasic endonuclease activity of APE1. J. Biol. Chem. 2006; 281:3889–3898. [PubMed: 16356936]
52. Hang B, Sagi J, Singer B. Correlation between sequence-dependent glycosylase repair and the thermal stability of oligonucleotide duplexes containing 1, N6-ethenoadenine. J. Biol. Chem. 1998; 273:33406–33413. [PubMed: 9837917]
53. Sagi J, Hang B, Singer B. Sequence-dependent repair of synthetic AP sites in 15-mer and 35-mer oligonucleotides: role of thermodynamic stability imposed by neighbor bases. Chem. Res. Toxicol. 1999; 12:917–923. [PubMed: 10525266]
54. Krosky DJ, Schwarz FP, Stivers JT. Linear free energy correlations for enzymatic base flipping: how do damaged base pairs facilitate specific recognition? Biochemistry. 2004; 43:4188–4195. [PubMed: 15065862]
55. Cao C, Jiang YL, Krosky DJ, Stivers JT. The catalytic power of uracil DNA glycosylase in the opening of thymine base pairs. J. Am. Chem. Soc. 2006; 128:13034–13035. [PubMed: 17017766]
56. Darwanto A, Theruvathu JA, Sowers JL, Rogstad DK, Pascal T, Goddard W III, Sowers LC. Mechanisms of base selection by human single-stranded selective monofunctional uracil-DNA glycosylase. J. Biol. Chem. 2009; 284:15835–15846. [PubMed: 19324873]
57. Erzberger JP, Barsky D, Scharer OD, Colvin ME, Wilson DM III. Elements in abasic site recognition by the major human and Escherichia coli apurinic/apyrimidinic endonucleases. Nucleic Acids Res. 1998; 26:2771–2778. [PubMed: 9592167]
58. Privalov G, Kavina V, Freire E, Privalov PL. Precise scanning calorimeter for studying thermal properties of biological macromolecules in dilute solution. Anal. Biochem. 1995; 232:79–85. [PubMed: 8600837]
59. Volker J, Blake RD, Delcourt SG, Breslauer KJ. High-resolution calorimetric and optical melting profiles of DNA plasmids: resolving contributions from intrinsic melting domains and specifically designed inserts. Biopolymers. 1999; 50:303–318. [PubMed: 10397791]
60. Volker J, Klump HH, Breslauer KJ. DNA metastability and biological regulation: conformational dynamics of metastable omega-DNA bulge loops. J. Am. Chem. Soc. 2007; 129:5272–5280. [PubMed: 17397164]
61. Marky LA, Breslauer KJ. Calculating thermodynamic data for transitions of any molecularity from equilibrium melting curves. Biopolymers. 1987; 26:1601–1620. [PubMed: 3663875]
62. Breslauer KJ. Extracting thermodynamic data from equilibrium melting curves for oligonucleotide order-disorder transitions. Methods Mol. Biol. 1994; 26:347–372. [PubMed: 7508801]

Research Highlights

- APE1 exhibits differential incision efficiency at AP sites in tandem repeat sequence elements
- APE1 incision efficiency is influenced by DNA sequence, damage arrangement, and positional context
- APE1 incision efficiency correlates with thermodynamic stability of substrate DNA
- Different genomic domains will be repaired with different efficiency or efficacy, giving rise to variability in damage accumulation and mutagenic potential

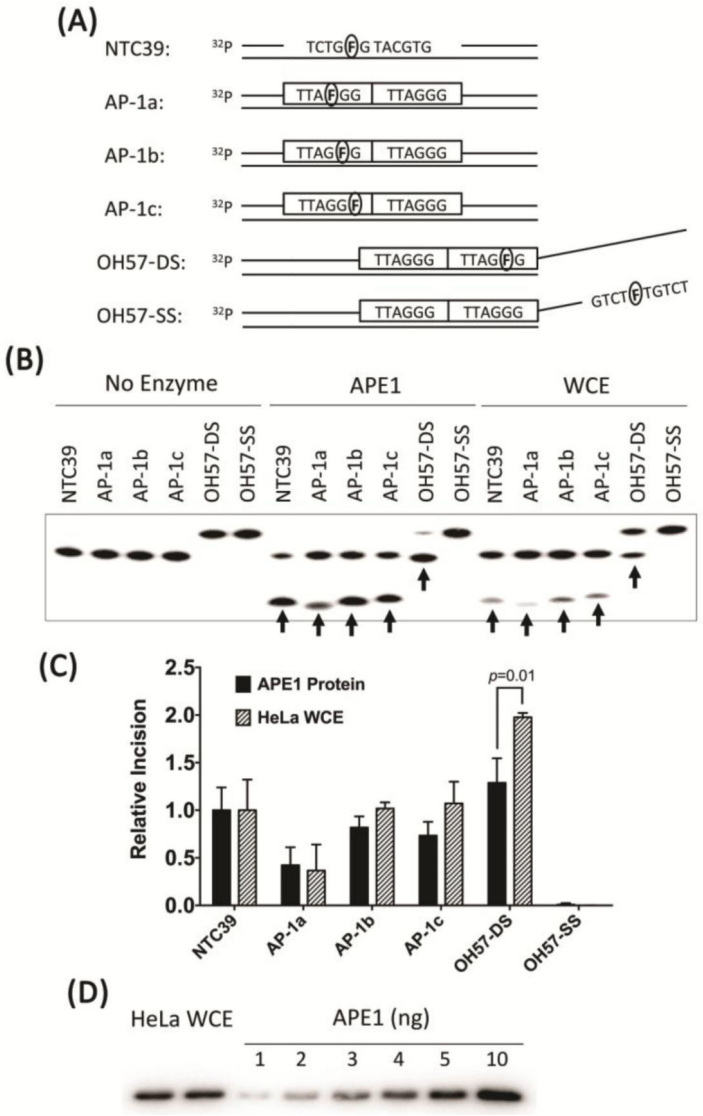

Figure 1.

Incision activity of APE1 at AP sites in telomeric repeats. (A) Composition of the AP site-containing telomeric and control substrates. Circled “F” represents the abasic site analogue, tetrahydrofuran (THF), and boxed sequence represents one telomeric repeat unit. Full nucleotide sequence information is provided in Table 2. Location of ^{32}P label is designated. (B) Representative gel image of AP site incision reactions. As indicated, reactions contained “No Enzyme”, purified human APE1 recombinant protein (200 pg, 0.56 nM), or HeLa WCE (300 ng) with 1 pmol of the designated substrate (100 nM). Arrow heads indicate the class II AP endonuclease incision products. (C) Incision activities for the different AP site-containing telomeric substrates relative to the NTC39 control. Results show relative values for purified APE1 (solid bars) and HeLa WCE (textured bars), considered independently. Reported are the averages and standard deviations of three data points. P values were determined via the student *t* test, with the only significant difference designated. (D) APE1 content in HeLa WCE (3 μg) as determined by Western blot analysis. The indicated amounts

of purified recombinant APE1 protein were loaded as a reference. Shown is a representative blot from three independent experiments.

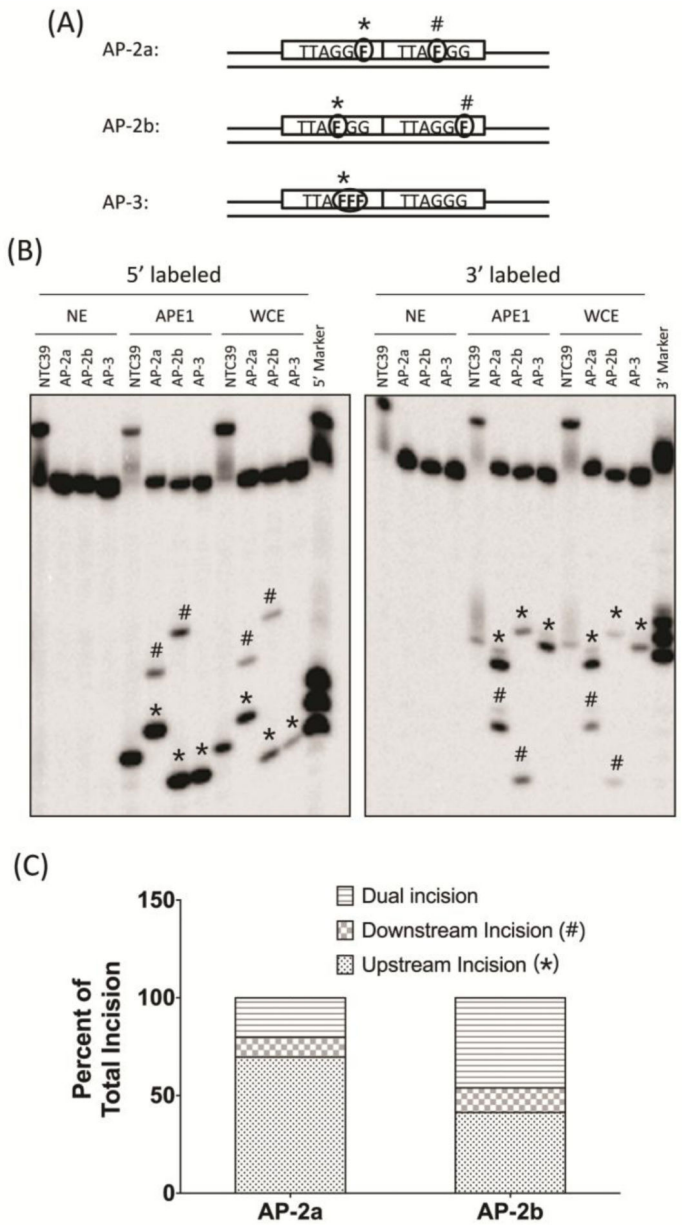

Figure 2.

Incision activity of APE1 at clustered AP sites in telomeric repeats. (A) Substrate composition of abasic site-containing telomeric repeat substrates. See Figure 1 for additional details. (B) Representative gel image of a typical AP site incision assay with either 5′-end labeled (left panel) or 3′-end labeled (right panel) oligomer substrates. Reactions were performed with no enzyme (NE), purified human APE1 (200 pg, 0.56 nM) or HeLa WCE (300 ng), and 1 pmol of the indicated substrate (100 nM). A mixture of AP site incision products from either 5′-end labeled or 3′-end labeled AP-1a, AP-1b and AP-1c substrates were loaded as molecular weight markers. (C) Distribution of incision sites for purified APE1 on the AP-2a and AP-2b substrates. For the 5′-end labeled substrates, the slower migrating product represents only downstream incision, whereas the faster migrating

product represents either upstream or dual incision. For the 3′-end labeled substrates, the slower migrating product represents only upstream incision, whereas the faster migrating product represents downstream or dual incision. From these data, we can determine the percentage distribution of upstream AP site incision only, downstream incision only, and dual incision, which is equal to the overlap in numbers for the differently labeled substrates. Results were obtained from at least three independent experiments. In all panels, the site of the upstream (or 5′) lesion or its incision product is designated with a "*", while the location of the downstream (or 3′) AP site or its product is identified with a "#".

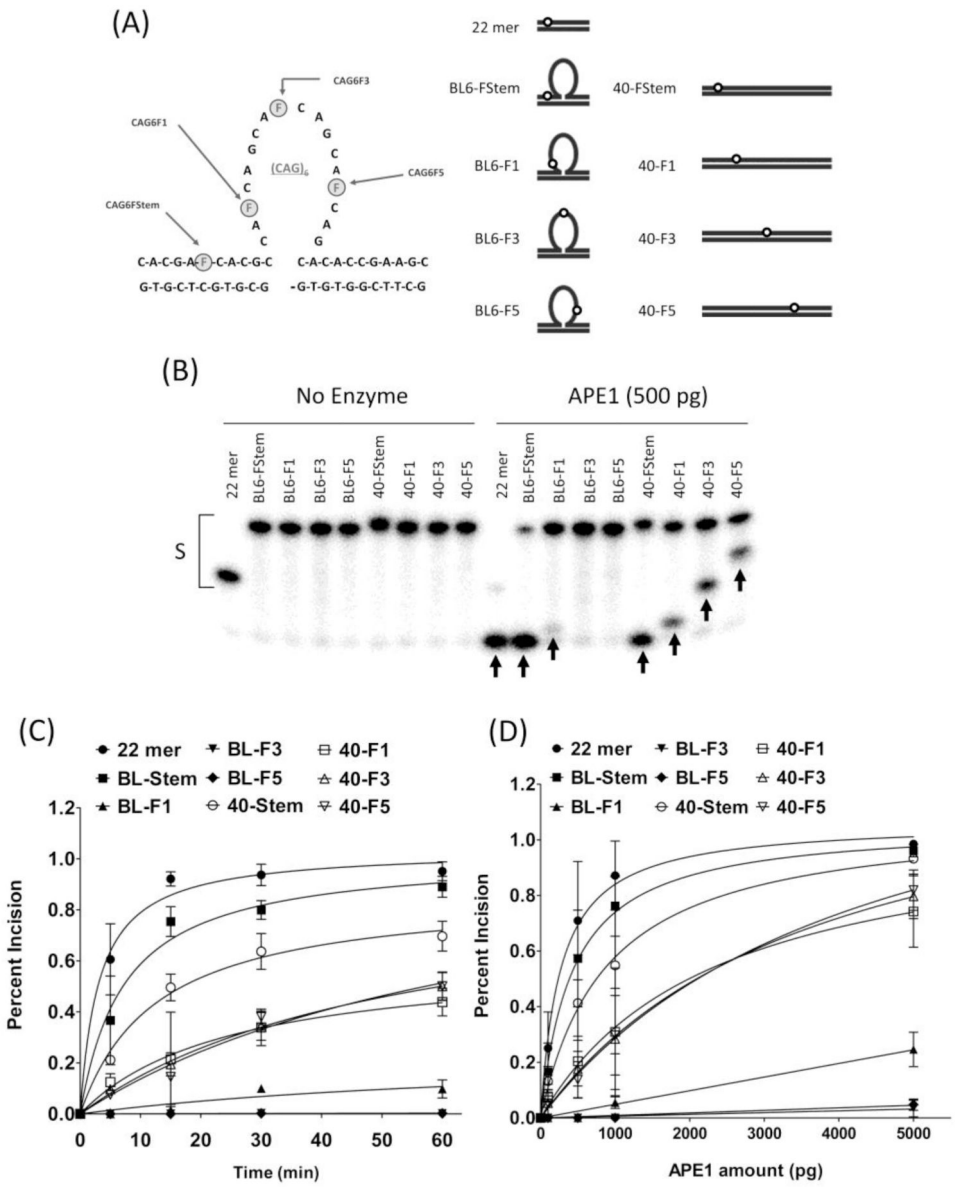

Figure 3.

Incision activity of APE1 at AP sites in the duplex or loop domain of TNR substrates. (A) TNR and control substrate composition. Nucleotide sequence and abasic site position of the $(CAG)_6$ bulge loop TNR substrates (left). Schematic of the various TNR and fully-duplex control substrates (right). The AP site analog, THF, is depicted by the circled “F” (left) or the open circle (right). Full nucleotide sequence information is provided in Table 2. (B) Representative gel image of an AP site incision assay with the various oligonucleotide substrates. Reactions contained either “No Enzyme” or purified human APE1 protein (500 pg, 1.4 nM) and 1 pmol of the indicated substrate (100nM, designed by “S”). Arrow heads indicate the products of AP endonuclease activity. (C) Time course (5, 15, 30 and 60 min) and (D) dose response (100, 500, 1000 and 5000 pg APE1, equal to 0.28, 1.4, 2.8 and 14 nM, respectively) reaction profiles. The data are from three independent experiments, and the graphs were generated by Prism Graphpad software.

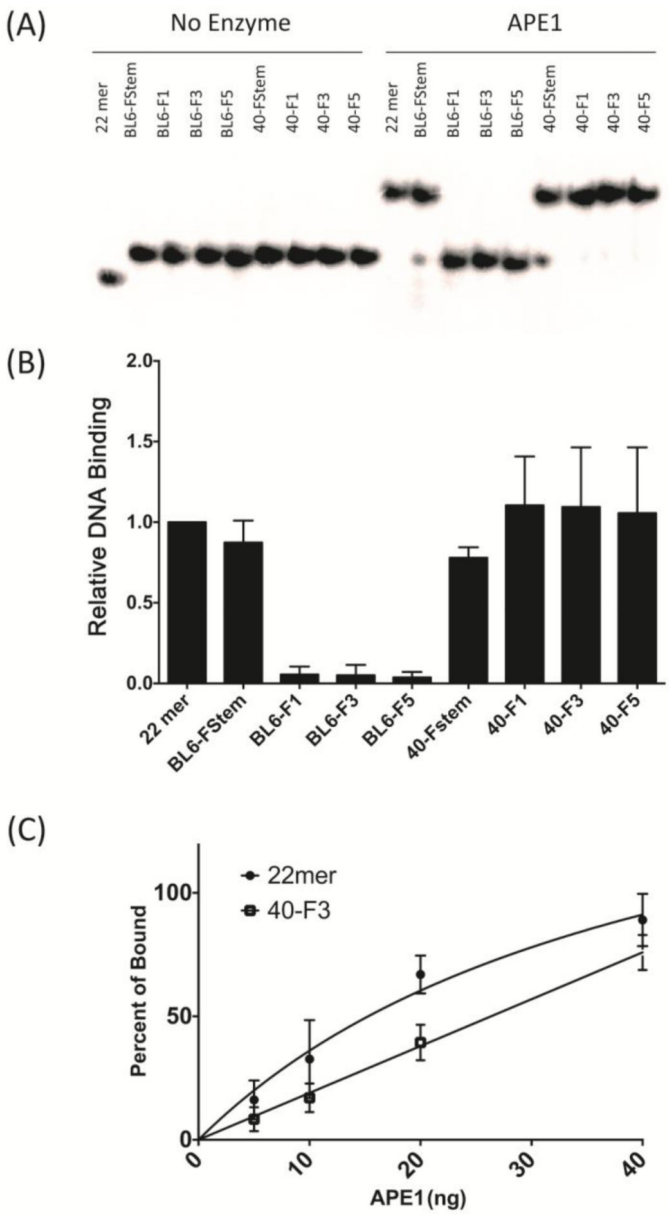

Figure 4.

DNA binding of APE1 to different TNR substrates. (A) Representative gel image of electrophoretic mobility shift assay. Binding reactions contained either “No Enzyme” or purified human APE1 (30 ng, 84 nM), and 100 fmol of the indicated substrate (10 nM), and were resolved on a native gel. (B) Relative APE1 binding to the different TNR substrates in comparison to the 22 mer control AP-DNA. (C) Binding affinity of APE1 for the 22 mer and 40-F3 substrates. Various amounts of APE1 (indicated) were incubated with 100 fmol of substrate (10 nM), and percentage of substrate bound was determined and plotted. Data represent the average and standard deviation of three independent experimental values.

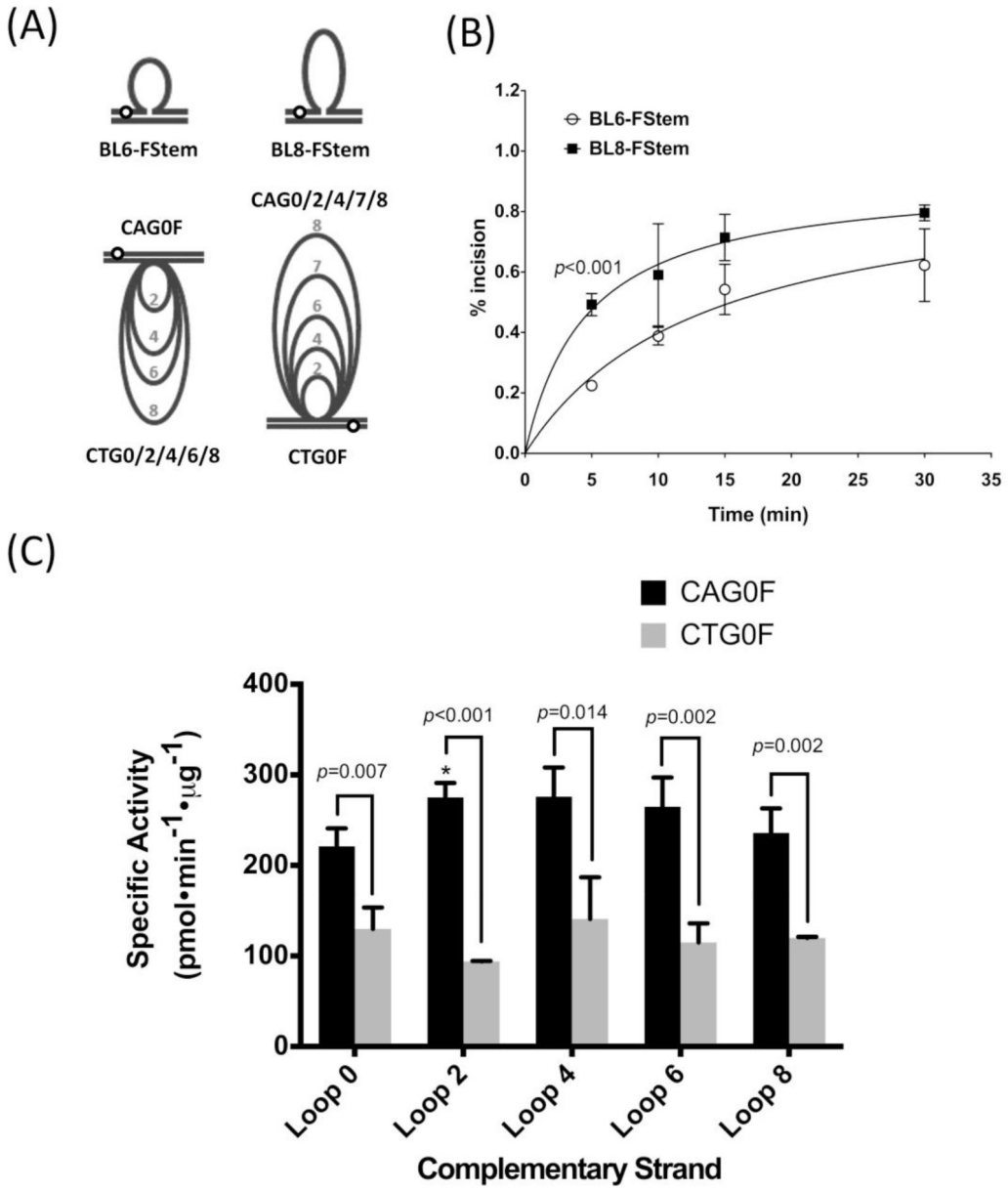

Figure 5.

Effect of loop size adjacent to AP site in duplex region on APE1 incision. (A) Schematic of the various loop-containing substrates. See Figure 3 for additional information, and Table 2 for full oligonucleotide composition. (B) Time course (5, 10, 15 and 30 min) reaction with the BL6-FStem and BL8-FStem TNR substrates. Reactions consisted of purified APE1 (100 pg, 0.28 nM) and 1 pmol of substrate (100 nM), and were incubated at 25 °C for the indicated time. (C) Relative incision efficiency of APE1 for the “CAG0F” (black bars) or “CTG0F” (grey bars) abasic site-containing oligonucleotide annealed to the indicated loop strand. Reactions were as above, and were performed at 25 °C for 15 min. The data represent the average and standard deviation of three independent experiments, and the graphs were generated by Prism Graphpad software. The asterisk (*) denotes that the

incision activities of CAG0F:CTG2 and CAG0F:CTG0 (22 mer) were significantly different ($p = 0.02$).

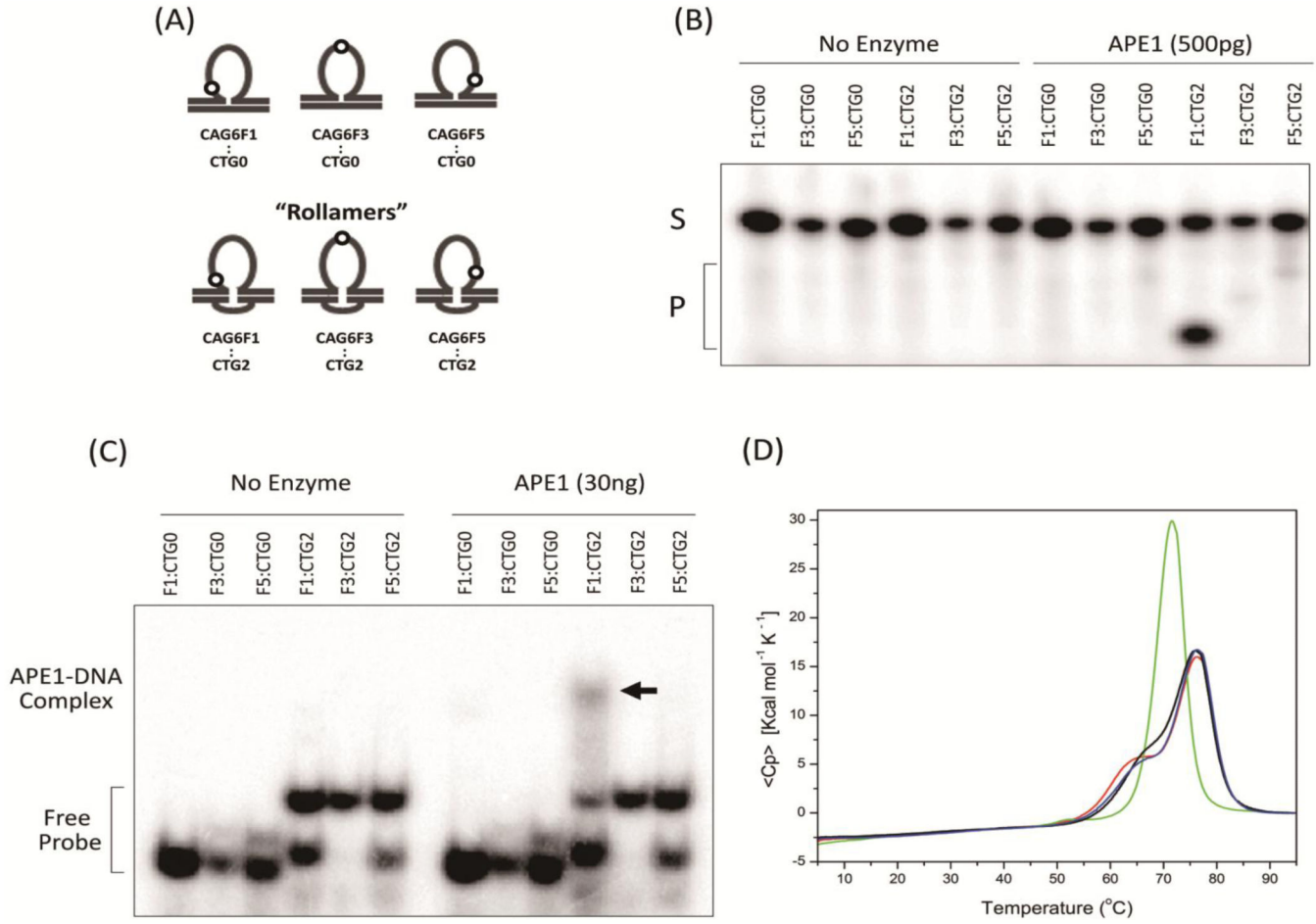

Figure 6.

Impact on APE1 incision of dynamic complementarity in AP site-containing TNR bulge loop. (A) Schematic of standard bulge loop TNR substrates (top) and comparable "rollamers" (bottom). See Figure 3 for additional information, and Table 2 for full oligonucleotide composition. (B) Representative gel image of an AP site incision assay using the substrates above. Reactions contained either "No Enzyme" or purified APE1 (500 pg, 1.4 nM) and 1 pmol of the indicated substrate (100 nM, designated as "S"). Incision products are indicated as "P". Note that "CAG6F1" is abbreviated "F1", etc. (C) Representative gel image of DNA binding assay. Reaction consisted of either "No Enzyme" or purified APE1 (30 ng, 84 nM) and 100 fmol of the indicated substrate (10 nM). Arrow indicates APE1-DNA complex, and the unbound, free probe is designated by the bracket. (D) Excess heat capacity traces for the parent rollamer (CAG6:CTG2 - in black) and the CAG6-F1:CTG2 (green), CAG6-F3:CTG2 (blue), and CAG6-F5:CTG2(red) rollamers in 10 mM cacodylate, 100 mM Na+ buffer. Note the altered shape of the CAG6F1:CTG2 melting curve (green), the only construct for which significant APE1 binding and processing activity was detected.

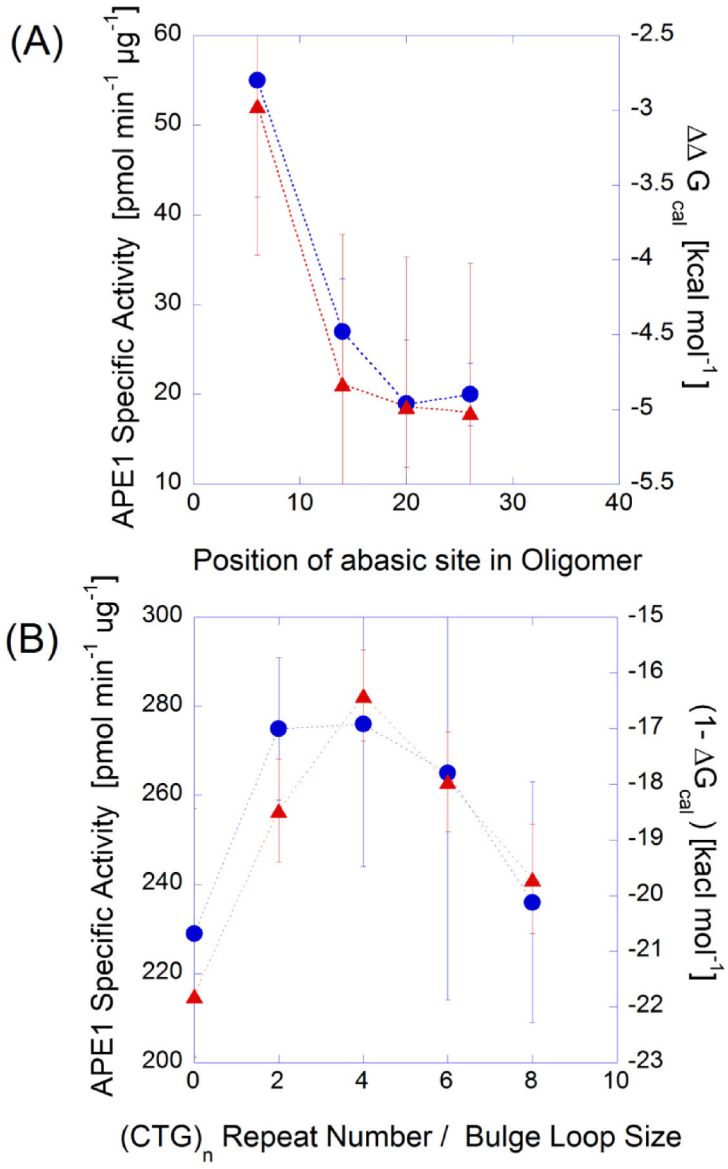

Figure 7.

Empirical correlation between substrate thermodynamic stability and APE1 incision activity. (A) Variation of APE1 incision activity with lesion position within the family of 40 mer duplexes (left axis, blue circles) shows the same trend as the lesion position dependence in duplex stability (ΔΔG) relative to the unmodified parent duplex (right axis, red triangles). (B) Dependence of APE1 incision activity CTG repeat bulge loop size downstream from the abasic lesion (left axis, blue circles) shows the same trend as the impact of the CTG bulge loop size on thermodynamic stability of the bulge loop construct (right axis, red triangles). Error bars are indicated in blue for enzyme activity and in red for free energy changes. Corresponding plots of APE1 cleavage activity versus free energy changes (not shown) can be fit to straight lines with R^2 correlations of 0.98 (panel A) and 0.8 (panel B).

Table 1

Specific activity of purified human APE1 against DNA substrates used in this study

Name of DNA substrate is indicated in left column, with the labeled and complementary strand designated (see Table 2 for nucleotide sequences).

Name	Labeled strand	Complementary strand	Specific activity ($pmol \cdot min^{-1} \mu g^{-1}$)
Telomeric substrates (37°C)			
NTC39	NTC39AP	NTC39C	265 ± 65
AP-1a	AP1a	TPL	81 ± 36
AP-1b	AP1b	TPL	157 ± 22
AP-1c	AP1c	TPL	140 ± 28
AP-2a	AP2a	TPL	155 ± 7.5 *
AP-2b	AP2b	TPL	150 ± 3.4 *
AP-3	AP3	TPL	116 ± 5.8
OH57-DS	OH57DS	OH57C	247 ± 49
OH57-SS	OH57SS	OH57C	1.6 ± 3.1
TNR substrates (25°C)			
22 mer	CAG0F	CTG0	229 ± 28
BL6-Fstem	CAG6Fstem	CTG0	77 ± 13
BL6-F1	CAG6F1	CTG0	2.3 ± 0.76
BL6-F3	CAG6F3	CTG0	0.19 ± 0.03
BL6-F5	CAG6F5	CTG0	0.93 ± 0.18
40-Fstem	CAG6Fstem	CTG6	55 ± 13
40-F1	CAG6F1	CTG6	27 ± 5.9
40-F3	CAG6F3	CTG6	19 ± 7.1
40-F5	CAG6F5	CTG6	20 ± 3.5
BL8-Fstem	CAG8Fstem	CTG0	197 ± 15
CAG0F:CTG2	CAG0F	CTG2	275 ± 16
CAG0F:CTG4	CAG0F	CTG4	276 ± 32
CAG0F:CTG6	CAG0F	CTG6	265 ± 51
CAG0F:CTG8	CAG0F	CTG8	236 ± 27
CTG0F:CAG0	CTG0F	CAG0	130 ± 24
CTG0F:CAG2	CTG0F	CAG2	94 ± 0.4
CTG0F:CAG4	CTG0F	CAG4	141 ± 46
CTG0F:CAG6	CTG0F	CAG6	115 ± 21
CTG0F:CAG7	CTG0F	CAG7	131 ± 14
CTG0F:CAG8	CTG0F	CAG8	120 ± 1.1
CAG6F1:CTG2	CAG6F1	CTG2	69 ± 6.3
CAG6F3:CTG2	CAG6F3	CTG2	1.5 ± 0.39
CAG6F5:CTG2	CAG6F5	CTG2	1.6 ± 0.73

*Specific activity derived from total incision of the multiple abasic sites in the substrate.

Table 2

Name and sequence of oligonucleotides uses in this study

Abasic site analog, THF or "F", is indicated in bold and underlined.

Oligo name	Sequence
Telomeric substrates	
NTC39AP	5′-GTGGATCCGTACTCTG**F**GTACGTGTCAACACGAATTCGA-3′
NTC39C	5′-TC GAATTCGTGTTGACACGTACC CAGAGTACGGATC CAC-3′
AP1a	5′-GTGGATCC GTACTTA**F**GGTTAGGGTTAACAC GAATTCGA-3′
AP1b	5′-GTGGATCC GTACTTAG**F**GTTAGGGTTAACAC GAATTCGA-3′
AP1c	5′-GTGGATCC GTACTTAGG**F**TTAGGGTTAACAC GAATTCGA-3′
AP2a	5′-GTGGATCC GTACTTAGGFTTA**F**GGTTAACAC GAATTCGA-3′
AP2b	5′-GTGGATCC GTACTTA**F**GGTTAGG**F**TTAACAC GAATTCGA-3′
AP3	5′-GTGGATCC GTACTTA**FFF**TTAGGGTTAACACGAATTCGA-3′
TPL*	5′-TC GAATTCGTGTTAACCCTAAC CCTAAGTACGGATC CAC-3′
OH57DS	5′-GTGGATCCGTACACACGAATTCGATGCTTAGGGTTAG**F**GTTATCTGTGTCTGTGTCT-3′
OH57SS	5′-GTGGATCCGTACACACGAATTCGATGCTTAGGGTTAGFGTTATCTGTGTCTFTGTCT-3′
OH57C#	5′-CCCTAACCCTAAGCATCGAATTCGTGTGTACGGATCCAC-3′
TNR substrates	
CAG0F	5′-CACGA**F**CACGCCACACCGAAGC-3′
CAG6Fstem	5′-CACGA**F**CACGCCAGCAGCAGCAGCAGCAGCACACCGAAGC-3′
CAG6F1	5′-CACGAGCACGCCA**F**CAGCAGCAGCAGCAGCACACCGAAGC-3′
CAG6F3	5′-CACGAGCACGCCAGCAGCA**F**CAGCAGCAGCACACCGAAGC-3′
CAG6F5	5′-CACGAGCACGCCAGCAGCAGCAGCA**F**CAGCACACCGAAGC-3′
CAG8Fstem	5′-CACGA**F**CACGCCAGCAGCAGCAGCAGCAGCAGCAGCACACCGAAGC-3′
CTG0F	5′-GCTTC**F**GTGTGGCGTGCTCGTG-3′
CTG0	5′-GCTTCGGTGTGGCGTGCTCGTG-3′
CTG6	5′-GCTTCGGTGTGCTGCTGCTGCTGCTGGCGTGCTCGTG-3′
CTG2	5′-GCTTCGGTGTGCTGCTGGCGTGCTCGTG-3′
CTG4	5′-GCTTCGGTGTGCTGCTGCTGCTGGCGTGCTCGTG-3′

Oligo name	Sequence
CTG8	5′-GCTTCGGTGTGCTGCTGCTGCTGCTGCTGCTGGCGTGCTCGTG-3′
CAG0	5′-CACGAGCACGCCACACC GAAG C-3′
CAG2	5′-CACGAGCACGCCAGCAGCACACCGAAGC-3′
CAG4	5′-CACGAGCACGCCAGCAGCAGCAGCACACCGAAGC-3′
CAG6	5′-CACGAGCACGCCAGCAGCAGCAGCAGCAGCACACCGAAGC-3′
CAG7	5′-CACGAGCACGCCAGCAGCAGCAGCAGCAGCAGCACACCGAAGC-3′
CAG8	5′-CACGAGCACGCCAGCAGCAGCAGCAGCAGCAGCAGCACACCGAAGC-3′

*TPL is the complementary strand for AP1a, AP1b, AP1c, AP2a, AP2b and AP3.

#OH57C is the complementary strand for OH57DS and OH57SS.